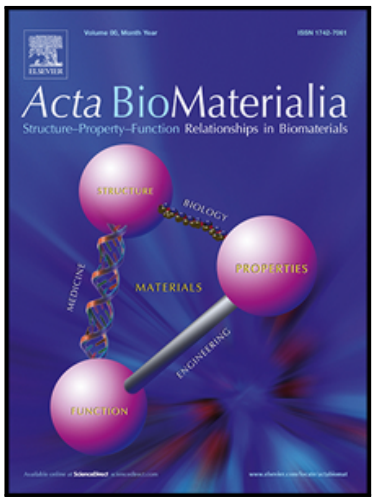

Bioengineering a humanized 3D tri-culture osteosarcoma model to assess tumor invasiveness and therapy response

Cátia F. Monteiro , Catarina A. Custódio , João F. Mano

PII: S1742-7061(21)00472-4
DOI: https://doi.org/10.1016/j.actbio.2021.07.034
Reference: ACTBIO 7497

To appear in: *Acta Biomaterialia*

Received date: 13 April 2021
Revised date: 14 July 2021
Accepted date: 15 July 2021

Please cite this article as: Cátia F. Monteiro , Catarina A. Custódio , João F. Mano , Bioengineering a humanized 3D tri-culture osteosarcoma model to assess tumor invasiveness and therapy response, *Acta Biomaterialia* (2021), doi: https://doi.org/10.1016/j.actbio.2021.07.034

Bioengineering a humanized 3D tri-culture osteosarcoma model to assess tumor invasiveness and therapy response

Cátia F. Monteiro, Catarina A. Custódio[*]*, João F. Mano*[*]

CICECO – Aveiro Institute of Materials, University of Aveiro, Department of Chemistry, Campus Universitário de Santiago, 3810-193 Aveiro, Portugal

[*] Corresponding authors:

João F. Mano

CICECO – Aveiro Institute of Materials, Department of Chemistry

University of Aveiro, Campus Universitário de Santiago

3810-193, Aveiro, Portugal

E-mail: jmano@ua.pt

Telephone: +351 234370733

Catarina A. Custódio

CICECO – Aveiro Institute of Materials, Department of Chemistry

University of Aveiro, Campus Universitário de Santiago

3810-193, Aveiro, Portugal

E-mail: catarinacustodio@ua.pt

Telephone: +351 234370733

Abstract

To date, anticancer therapies with evidenced efficacy in preclinical models fail during clinical trials. The shortage of robust drug screening platforms that accurately predict patient's response underlie these misleading results. To provide a reliable platform for tumor drug discovery, we herein propose a relevant humanized 3D osteosarcoma (OS)

model exploring the potential of methacryloyl platelet lysates (PLMA)-based hydrogels to sustain spheroid growth and invasion. The architecture and synergistic cell-microenvironment interaction of an invading tumor was recapitulated encapsulating spheroids in PLMA hydrogels, alone or co-cultured with osteoblasts and mesenchymal stem cells. The stem cells alignment toward OS spheroid suggested that tumor cells chemotactically attracted the surrounding stromal cells, which supported tumor growth and invasion into the hydrogels. The exposure of established models to doxorubicin revealed an improved drug resistance of PLMA-based models, comparing with scaffold-free spheroids. The proposed OS models highlighted the feasibility of PLMA hydrogels to support tumor invasion and recapitulate tumor-stromal cell crosstalk, demonstrating the potential this 3D platform for complex tumor modelling.

Statement of Significance

Cell invasion mechanisms involved in tumor progression have been recapitulated in the field of 3D *in vitro* modeling, leveraging the great advance in biomimetic materials. In line with the growing interest in human-derived biomaterials, the aim of this study is to explore for the first time the potential of methacryloyl platelet lysates (PLMA)-based hydrogels to develop a humanized 3D osteosarcoma model to assess tumor invasiveness and drug sensitivity. By co-culturing tumor spheroids with human osteoblasts and human mesenchymal stem cells, this study demonstrated the importance of the synergistic tumor cell-microenvironment interaction in tumor growth, invasion and drug resistance. The established 3D osteosarcoma model highlighted the feasibility of PLMA hydrogels as a relevant 3D platform for complex tumor modelling.

Keywords: 3D *in vitro* tumor model, osteosarcoma, human platelet lysates, co-culture, drug screening

1. Introduction

Osteosarcoma (OS) is the most common primary malignant bone tumor that exhibit high prevalence in children and adolescents [1]. This osteogenic sarcoma is a highly heterogeneous tumor and mainly arises in regions of faster bone turnover with frequent incidence in the distal femur, proximal tibia and proximal humerus [2,3]. Despite the advances in oncologic diagnosis and treatment, the poor-prognosis, low effectiveness of the available therapies, high rate of recurrence, micrometastasis development (typically pulmonary), and chemoresistance are the major reasons that hamper better clinical outcomes [4,5]. Even though several potential drug candidates have been identified, standard chemotherapy regimen and patient outcome is stagnated since late 1970s [6,7]. There is a cumulating evidence that the high failure rate of oncology drug discovery in clinical trials is associated to the non-predictivity of the current preclinical *in vitro* models [8]. The complexity and dynamism of tumor microenvironment in terms of cellular milieu and surrounding extracellular matrix is recognized as crucial aspects that *in vitro* models should recapitulate in order to improve OS therapy development [9–11].

Traditionally, cancer biology research and drug discovery rely on two-dimensional (2D) *in vitro* cell cultures and *in vivo* animal models to study tumor growth, metastasis and drug response. In 2D models, the lack of native-like cell-cell and cell-extracellular matrix (ECM) interactions results in different gene and protein expression and cellular behavior [12]. Motivated by these drawbacks, great efforts have been made exploring three-dimensional (3D) *in vitro* cell culture systems to closely reproduce the tumor pathophysiology and, by this way, properly identify effective drug candidates and predict patient's response [13,14]. The tridimensionality of these systems offers biochemical and mechanical tissue-specific cues that preserve the native

cell morphology and polarization [15]. In this environment, tumor cells can self-organize into 3D structures, favoring the acquisition of a malignant phenotype characterized by invasive processes and drug resistance [16,17]. The surrounding cellular microenvironment is also actively involved in tumor cell behavior and chemoresistance by juxtacrine or paracrine tumor-stromal cell crosstalk that regulate ECM protein and soluble factors secretion [18,19]. In this context, human mesenchymal stem cells (hMSCs) have been considered as pivotal players in the ECM remodeling, suppression of the immune response, epithelial-to-mesenchymal transition of tumor cells and consequent metastasis [20–23]. The recognition of their pro-tumorigenic role in tumor growth mechanisms has been prompted their use for cell-mediated therapy purposes, including in OS [21,24–26].

The tumor microenvironment is further characterized by a phenotypic heterogeneity associated with biochemical gradients of oxygen, pH and nutrients [27]. The recognition of this distinct phenotype as a key player in tumor drug sensitivity have fostered the development of 3D models with closest tumor morphology, named multicellular tissue spheroids (MCTS), and stimulating the search for high-throughput platforms for screening and validation of new therapies [28]. Indeed, several studies have reported that 3D OS models based on spheroids are usually more resistant to therapies than their 2D counterparts [29–33]. More recently, the embedding of an OS spheroid into an ECM-like matrix, such as a hydrogel, seems to be a promising strategy to recreate the early metastatic processes in a more realistic way, once it is provided an appropriate scaffold for tumor cells to invade [34,35]. The incorporation of stromal cells into that exogenous matrix have been recapitulating the tumor-stromal cells interactions responsible for tumor growth suppression or promotion and acquisition of drug

resistance mechanisms [36–38]. However, these biomaterials-based approaches for osteosarcoma tumor modelling is still very limited.

Recent advances in 3D *in vitro* OS models have been boosted by the progress in the field of functional and biomimetic materials both of natural or synthetic origin to study cell behavior in response to materials' biochemical and biophysical cues [39,40]. Invasion models based on reconstituted basement membrane (rBM) of murine Engelbreth-Holm-Swarm (EHS) sarcoma and type I collagen have provided fundamental insights in this field [41–43]. However, there is a growing interest in human-derived biomaterials, particularly in blood plasma proteins and growth factors, to develop humanized 3D *in vitro* models [44]. Methacryloyl platelet lysates (PLMA) is a recently developed biomimetic material of human origin that exhibit highly tunable mechanical properties, demonstrating to support human cells proliferation and the invasive phenotype of cell spheroids [35,45]. In this context, we herein report the use of this ECM-mimicking matrix highly rich in physiologically native proteins to establish a 3D tri-culture model of osteosarcoma. For that, the culture of tumor spheroids alone or in combination with human osteoblasts and human bone-marrow mesenchymal stem cells (hBM-MSCs) is expected to create a bone tumor-like microenvironment (Figure 1). It is anticipated that stromal cells will provide a more realistic environment, interacting with invasive tumor cells and improving their resistance to drug treatment. Taking OS as a case-of-study, the aim of the presented work is to validate this human-derived ECM as an innovative 3D platform for the development of complex tumor models to understand the influence of tumor-stromal cell crosstalk on tumor mass growth, invasion and response to therapeutics.

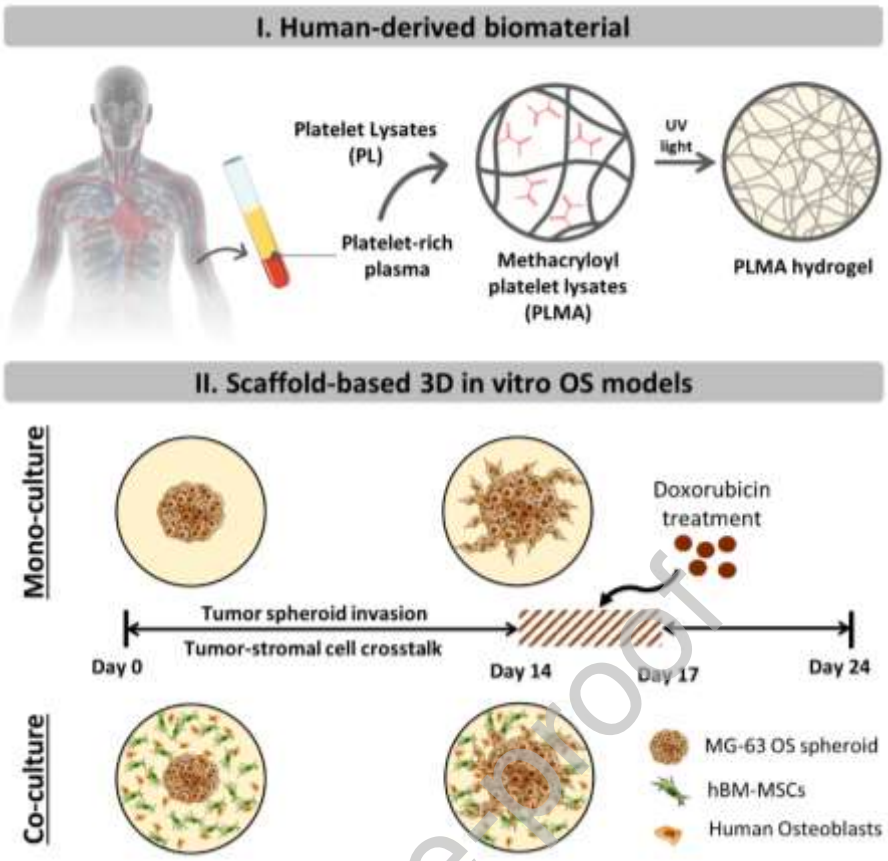

Figure 1. Schematic representation of human methacryloyl platelet lysates (PLMA) hydrogels production and scaffold-based 3D *in vitro* OS models establishment. (I) Platelet lysates (PL) derived from human platelet-rich plasma is chemically modified with functional moieties that photo-crosslink by ultraviolet (UV) irradiation. (II) This human-derived biomaterial is subsequently used to establish 3D OS mono- and co-culture models. The chemoresistance to doxorubicin treatment is evaluated after a culture period in which tumor cells are allowed to invade the PLMA hydrogel and synergistically interact with stromal cells.

2. Materials and Methods

2.1. Synthesis of methacryloyl platelet lysates

Methacryloyl platelet lysates (PLMA) were synthesized as previously reported, using human platelet lysates (STEMCELL Technologies, Canada) [45]. Briefly, PLMA

of low-degree of modification (PLMA100) was synthesized through a reaction with methacrylic anhydride (94% (MA), Sigma-Aldrich, USA) in a ratio of 100:1 (v/v), at room temperature (RT) under constant stirring. Afterwards, PLMA was purified against deionized water by dialysis with Float-A-Lyzer G2 Dialysis Device 3.5-5 kDa (Spectrum, USA). The PLMA solution was sterilized with a low protein retention 0.2 µm filter (Sigma-Aldrich), frozen with liquid nitrogen, lyophilized (LyoQuest Plus Eco) and stored at 4°C until further use.

2.2. Cell culture

Human bone-marrow mesenchymal stem cells (hBM-MSCs, American Type Culture Collection, ATCC, USA) and MG-63 cell line (European Collection of Authenticated Cell Cultures, ECACC, UK) were cultured in Minimum Essential Medium Alpha (α-MEM, Thermo Fisher Scientific, USA) supplemented with sodium bicarbonate (2.2 g L^{-1}, Sigma-Aldrich), 10% (v/v) heat-inactivated fetal bovine serum (FBS, Thermo Fisher Scientific) and 1% (v/v) antibiotic/antimycotic (10,000 units mL^{-1} of penicillin, 10,000 µg mL^{-1} of streptomycin, and 25 µg mL^{-1} of Amphotericin B, Thermo Fisher Scientific). Fetal human osteoblasts (FhOB, Cell Applications, Inc., USA) were cultured in 1:1 ratio of human Osteoblast Growth Medium (hOGM, Cell Applications, Inc., Sigma-Aldrich) with 10% (v/v) heat-inactivated FBS and 1% (v/v) antibiotic/antimycotic and Dulbecco's Modified Eagle's Medium/Nutrient Mixture F-12 Ham (DMEM/F-12, Sigma-Aldrich) supplemented with sodium bicarbonate (1.2 g L^{-1}), bovine serum albumin (BSA, 5 g L^{-1}, Sigma-Aldrich), L-ascorbic acid 2-phosphate (5 mg mL^{-1}, Cayman Chemical, USA), 10% (v/v) heat-inactivated FBS and 1% (v/v) antibiotic/antimycotic. All cells were cultured in T-flasks, maintained under 5% CO_2

atmosphere at 37°C (standard cell culture conditions) and passaged at about 80% confluence. The medium was replaced every 2 to 3 days.

2.3. Generation of fluorescence protein-expressing cells

In order to achieve endogenous cell fluorescence, MG-63 and hBM-MSCs were stably transduced with lentiviruses expressing red fluorescence protein (CMV-RFP, Cellomics Technology, USA) and green fluorescence protein (CMV-GFP, Vigene Biosciences, USA), respectively. The cells were transduced at a multiplicity of infection (MOI) of 10 and incubated in culture medium for 12h in the presence of polybrene (6 μg mL^{-1}, Sigma-Aldrich). Three days after transduction, fluorescence protein-expressing cells were selected through a treatment with puromycin (2 μg mL^{-1}, STEMCELL Technologies, Canada) in culture medium.

2.4. Generation of MG-63 multicellular tumor spheroids

MG-63 or MG-63-RFP cells were detached with 0.25% trypsin/EDTA (Gibco, Thermo Fisher Scientific) and re-suspended in α-MEM culture medium. MG-63 spheroids were generated in 96-well round-bottom ultra-low attachment plates (Corning, Thermo Fisher Scientific, USA) at a density of 12,000 cells in culture medium (150 μL). Seeded cells were centrifuged at 500g for 10 minutes and incubated for 72 hours at standard cell culture conditions. Generated spheroids were imaged using an inverted light microscope (Primostar, Carl Zeiss, Germany) with ZEN Imaging software.

2.5. 3D osteosarcoma models establishment

2.5.1. Scaffold-free model – Spheroid: MG-63 spheroids formed for 72h were maintained in culture for additional 24 days and the culture medium was replaced every 2 to 3 days.

2.5.2. Scaffold-based model - Mono-culture: MG-63 generated spheroids were randomly chosen for embedding into a PLMA hydrogel precursor solution at 15% (w/v) prepared by dissolving lyophilized PLMA in a sterilized solution of 0.5% (w/v) 2-hydroxy-4'-(2-hydroxyethoxy)-2-methylpropiophenone (Sigma-Aldrich) in phosphate buffered saline (PBS), Sigma-Aldrich, USA). μ-Slide Angiogenesis plates (ibidi, Germany) were used to embed and culture the spheroids into PLMA hydrogel. For 3D spheroid embedding, a first layer of PLMA (5 μL) was made by photopolymerization using ultraviolet (UV) irradiation (0.095 W cm^{-2}, 320-500nm filter, Omnicure-S2000, Excelitas Technologies Corp., USA) during 15s, performing a semi-crosslinking. The spheroid was placed on the top of the first layer, as much as possible in the center of the well, and a second layer (5 μL) was formed at the same conditions, during 60s. Then, α-MEM was added to each well and the samples were incubated for 24 days at standard cell culture conditions. The culture medium was replaced every 2 to 3 days.

2.5.3. Scaffold-based model - Co-culture: hBM-MSCs and FhOBs until passage 8 were detached with 0.25% trypsin/EDTA and re-suspended in their culture medium. A cell density of 1:3:4 of MG-63:hBM-MSCs:FhOBs was selected for the co-culture studies, taking into account the MG-63 cell number aforementioned for spheroid generation. The corresponding cell density of stromal cells was re-suspended in PLMA hydrogel precursor solution at 15% (w/v) and the hydrogel polymerization, incorporating the MG-63 spheroid, was performed as described in the previous subsection ("Scaffold-based model - Mono-culture"). hBM-MSCs and FhOBs were separately cultured, at similar cell density, to compare their viability with the co-culture

setting. In order to monitor stromal cell organization inside the hydrogel, the lentivirus transduced cells (MG-63-RFP and hBM-MSC-GFP) were used following the above-described procedure. Throughout the assays, the co-culture model was cultured in α-MEM:hOGM:DMEM/F-12 (2:1:1) culture medium at standard conditions. The culture medium was replaced every 2 to 3 days.

2.6. Stromal cell orientation angles

The 3D OS models were monitored overtime via optical contrast microscopy by using an upright widefield microscope and under a scanning confocal microscope (LSM 880 Airyscan, Carl Zeiss, Germany) with ZEN Imaging software, and the acquired images were processed using ImageJ software. The spheroid center was estimated, and the stromal cells evidently stretched, with a defined orientation, outside the invasive area were identified. Cell orientation angle relative to spheroid center was measured using the Angle tool, and the cellular alignment data was then graphed as polar histograms in MATLAB. The distance from each analyzed stromal cell to spheroid center was also measured.

2.7. Doxorubicin diffusivity

The diffusivity of doxorubicin (DOX) into PLMA hydrogels was assessed using µ-slide Chemotaxis plates (ibidi, Germany). PLMA hydrogel was photopolymerized in the central channel as previously described and hydrated overnight with cell culture medium. A 100 µM DOX solution in cell culture medium was introduced into one of the reservoirs and DOX diffusivity was followed by fluorescence imaging in a confocal microscope, maintaining laser properties and z-axis coordinates. Fluorescence intensity

was measured using the "Plot profile" function of ImageJ software and the data was analyzed in GraphPah Prism 7.00 software.

2.8. Doxorubicin dose-response testing

To determine the IC_{50}-value of the established 3D OS models, a dose-response test using DOX was performed. After 14 days in culture, the 3D models were exposed to a range of DOX concentrations during 72h, at standard culture conditions. Samples cultured without DOX exposure were also included as controls. Serial dilutions of this anti-cancer drug were prepared in the appropriate culture medium (α-MEM for mono-culture models and α-MEM:hOGM:DMEM/F-12 (2:1:1) for co-culture model), in a range of 0.05 to 100 μM. After a 3-day drug treatment, the samples were maintained in culture for 7 days with fresh culture medium, performing a total of 24 days of culture. At day 24, the samples were washed with PBS and incubated in 0.25% trypsin/EDTA for 1h, at standard culture conditions, in order to degrade PLMA matrix. Thereafter, an equal amount of culture medium was added. The cell metabolic activity was then measured incubating the samples with CellTiter 96® AQ_{ueous} One Solution (Promega, USA) for 6h, following manufacturer instructions. The quantification of formazan product was performed by measuring the absorbance at 490 nm in a microplate reader (Synergy HTX, Biotek, USA). The IC_{50}-values were calculated fitting a non-linear regression of variable slope with four parameters of "log(inhibitor) vs. response" using the GraphPah Prism 7.00 software, with a confidence interval of 95%, where the following equation were used to fit the experimental results (Equation (1)):

$$Y=\text{Bottom}+\frac{\text{Top-Bottom}}{1+10^{\text{logIC50-X}}*\text{HillSlope}} \qquad (1),$$

where Top and Bottom are the plateaus in Y axis, IC50 is the drug concentration that gives a response halfway between Bottom and Top, and HillSlope is the steepness of the family of curves.

2.9. Cytotoxicity test with doxorubicin

The effect of DOX treatment in cell viability, morphology, spheroid area and cell invasion were assessed by exposing the 3D models to a DOX concentration of 1.1 μM, which was chosen because it is a doxorubicin concentration corresponding to the IC_{50}-value of the scaffold-free spheroid model. As previously described, a 3-day DOX treatment after 14 days in culture was performed and the samples were maintained in culture with fresh culture medium for 7 days after treatment. Control groups, without doxorubicin treatment, were also included.

2.9.1. Metabolic activity quantification: Cell metabolic activity of control and DOX-treated conditions was quantified as described before, using the CellTiter 96® AQ_{ueous} One Solution. Briefly, at 24 days of culture, samples were washed with PBS, digested with 0.25% trypsin/EDTA for 1h and then incubated with the reagent solution for 6h, according to manufacturer instructions. Thereafter, absorbance at 490 nm was measured using a microplate reader.

2.9.2. Cell viability, morphology, and spatial organization: Cell viability of the spheroids after 3 days of formation and the 3D OS models at day 14 (before drug treatment) and 24 (10 days after drug treatment) was assessed by a fluorescence live/dead assay. The samples were incubated in a solution of 1:100 of Calcein AM solution (4 mM) in dimethyl sulfoxide (DMSO, Life Technologies, Thermo Fisher Scientific) and 1:200 of Propidium Iodide (PI, Thermo Fisher Scientific) in PBS, at

standard cell culture conditions for 2 hours. After washing with PBS, the samples were observed under a widefield microscope (Axio Imager M2, Carl Zeiss, Germany).

Cell morphology assessment through DAPI/Phalloidin staining was performed at the same time points. OS models were washed with PBS and fixed in a solution of 4% (v/v) formaldehyde (Sigma-Aldrich) in PBS during at least 2 hours. Before staining, samples were permeabilized with 0.5% (v/v) Triton X-100 (Sigma Aldrich) for 30 minutes and blocked with 5% (v/v) FBS in PBS for 1 hour at RT. For phalloidin staining (Phalloidin-iFluor 594 Reagent, ab176757, abcam, UK), the original solution was diluted 1:8 in PBS and the hydrogels were incubated at RT for 90 minutes and then washed with PBS. Afterwards, a DAPI (4',6-diamidino-2-phenylindole, Thermo Fisher Scientific) solution diluted 1:1000 in PBS was used to incubate the hydrogels during 30 minutes at RT. After several PBS washes, the 3D models were observed under a scanning confocal microscope (LSM 880 Airyscan, Carl Zeiss, Germany).

The co-culture models constituted by lentivirus transduced cells were monitored using a scanning confocal microscope (LSM 880 Airyscan, Carl Zeiss, Germany). At day 14 and 24 of culture, these OS co-culture models were fixed in a solution of 4% (v/v) formaldehyde, permeabilized with 0.5% (v/v) Triton X-100, blocked with 5% (v/v) FBS in PBS and stained with a DAPI solution following the procedures above-described. The samples were visualized under a widefield microscope (Axio Imager M2, Carl Zeiss, Germany). The actin filaments of co-culture model samples at the 24 days of culture were also stained with phalloidin (Phalloidin-iFluor 405 Reagent, ab176752, abcam, UK). The original solution was diluted 1:200 in PBS, the hydrogels were incubated at RT for 90 minutes and then washed with PBS. Samples were observed under a scanning confocal microscope.

2.9.3. *Assessment of bone-related matrix deposition by histology and immunohistochemistry:* 3D OS model samples were collected after 14 and 24 days of culture, washed in PBS and fixed in 4% (v/v) formaldehyde in PBS during at least 2 hours. Samples were then dehydrated in ethanol, cleared in xylene, paraffin-embedded and cross-sectioned (5 µm) using a microtome (HM 340E Electronic Rotary Microtome, Thermo Fischer Scientific). Before histological and immunohistochemical staining, the sections were deparaffinized and rehydrated.

For hematoxylin and eosin (H&E) staining, sections were immersed in Mayer's hematoxylin (Sigma Aldrich) solution for 10 minutes, washed in distilled water, following by immersion in eosin Y (Sigma Aldrich). To evaluate the presence of calcium deposits, the sections were stained with 2% (w/v) Alizarin Red solution (Sigma Aldrich) for 30 minutes. Collagens deposition was assessed by staining with Aniline Blue solution (Sigma Aldrich) for 5 minutes and washed with 1% (v/v) acetic acid. All histological samples were dehydrated, immersed in xylene and mounted (DPX Mountant, Sigma Aldrich) before visualization by phase contrast microscopy with Axio Imager M2.

Osteopontin (OP) and osteocalcin (OC) production was assessed after antigen retrieval in 10mM sodium citrate buffer (Sigma Aldrich) at 95-100ºC for 20 minutes. The slides were cool down for 20 minutes and the sections were permeabilized with 0.5% Triton X-100 for 5 minutes, blocked with 5% FBS (v/v) in PBS for 30 minutes and incubated overnight in a humidified chamber at 4ºC with the primary antibodies rabbit anti-human osteopontin (1:1000 in 5% FBS (v/v) in PBS, Sigma Aldrich) and rabbit anti-human osteocalcin (1:1000 in 5% FBS (v/v) in PBS, Sigma Aldrich). After washing with PBS, samples were incubated with the secondary antibody anti-rabbit AlexaFluor 647 (1:1000 in FBS (v/v) in PBS, Thermo Fisher Scientific) for 1h at RT,

and then counterstained with DAPI (1:1000) for 5 minutes at RT. The samples were visualized by fluorescence microscopy (Axio Imager M2).

2.9.4. Spheroid area and cell invasion length measurement: Raw images obtained by optical contrast microscopy were processed using the Image Processing tool of ZEN Image software. Quantification of spheroid area was performed using an open-source MATLAB-based high-throughput image analysis software, SpheroidSizer. This software applies an adapted active contour algorithm suitable to automatically or manually measure spheroid size, excluding the invasive branches [46]. Cell invasion length around spheroid was quantified using ImageJ software. For the co-culture model, tumor cell invasion length was measured in fluorescence microscopy images, considering the RFP-stained tumor cells. The tumor spheroid center was estimated as the center of the circumference that better fits the area corresponding to the compact region of the spheroid, excluding the invasive branches. The length from the estimated spheroid center to the longer invasive branch of each sample – the invasion radius – was measured. The invasion length of each time-point was normalized to the spheroid radius measured at day 0 by using Equation (2):

$$\text{Invasion length} = \text{Invasion radius} - \text{Spheroid radius}_{\text{Day0}} \quad (2),$$

where $\text{Spheroid radius}_{\text{Day 0}}$ is the obtained value for the radius from the spheroid area measured at day 0, considering the spheroid delimitation a circumference. All data was converted from the acquired pixels (px) to micrometers (μm).

2.10. Statistical analysis

All data were statistically analyzed using the GraphPah Prism 7.00 Software and are expressed as mean ± standard deviation (SD) or mean ± standard error of the mean (SEM) of at least 3 independent experiments. The distribution of the initial spheroid

sizes was analyzed with the D'Agostino-Pearson normality test. For cell metabolic activity and invasion length data, statistical significance between the different groups was identified using two-way ANOVA analysis of variance combined with Tukey's multiple comparisons test, and the differences were considered significant when $p < 0.05$.

3. Results

3.1. Establishment of 3D mono- and co-culture models

Three configurations of *in vitro* OS models were established culturing MG-63 tumor spheroids (i) in a scaffold-free manner, and encapsulated into PLMA hydrogels (ii) alone or (iii) surrounded by dispersed hBM-MSCs and FhOBs (Figure 1). MG-63 spheroids were generated using 96-well round-bottom ultra-low attachment plates, a robust high-throughput platform that uses the forced-floating methodology for MCTS formation. The reproducibility of spheroids generation was confirmed by size normality distribution analysis (Figure S1A,B). The optimal seeding density was established at 12,000 cells/spheroid, producing tightly compacted spheroids with (464.4 ± 4.8) μm in diameter at 72h. Fluorescence microscopy images of Calcein-AM and PI stains confirmed the formation of a necrotic core surrounded by a proliferative zone, a condition that supports the presence of physiological gradients and validates their feasibility to be used throughout this study (Figure S1C).

Aiming to establish the 3D co-culture OS model for this study, the ideal cell-to-cell ratio was defined as the condition in which tumor cells in the spheroid were able to invade the PLMA matrix and the stromal cells could synergistically interact with tumor cells, migrating towards them. Hence, the cell-to-cell ratio for this study was established as the tri-culture of the MG-63 tumor spheroid with hBM-MSCs and FhOBs in the ratio

1:3:4. At this condition, a tumor cell outward migration and its interplay with surrounded stromal cells resulted in the formation of invasive branches as verified in fluorescence images of samples obtained from lentivirus transduced cells (Figure 2A, S2 and S3). Moreover, hBM-MSCs stretched inside the matrix, forming a complex network of interacting tumor and hBM-MSCs cells (Figure S3 and Movie S1). FhOBs maintained their native cuboidal-to-round shape phenotype (Figure S2B,C). The three 3D OS model settings herein established were monitored by phase contrast microscopy over the 24 days of culture (Figure S2A and S4). Cell orientation analysis showed that stretched stem cells randomly oriented at 3 days of culture were chemotactically attracted by tumor cells in the spheroids, promoting their orientation toward spheroid center overtime (Figure 2B,C and S5). This evidence was also confirmed by fluorescence microscopy images of hBM-MSC-GFP in the co-culture model including fluorescent protein-transduced cells (Figure 2B). Interestingly, stem cells at the hydrogel periphery also stretched in spheroid center direction, demonstrating that they react to paracrine signals released by tumor cells (Figure S5). When hBM-MSCs were cultured alone inside PLMA hydrogels, no specific cell orientation was observed (Figure S6).

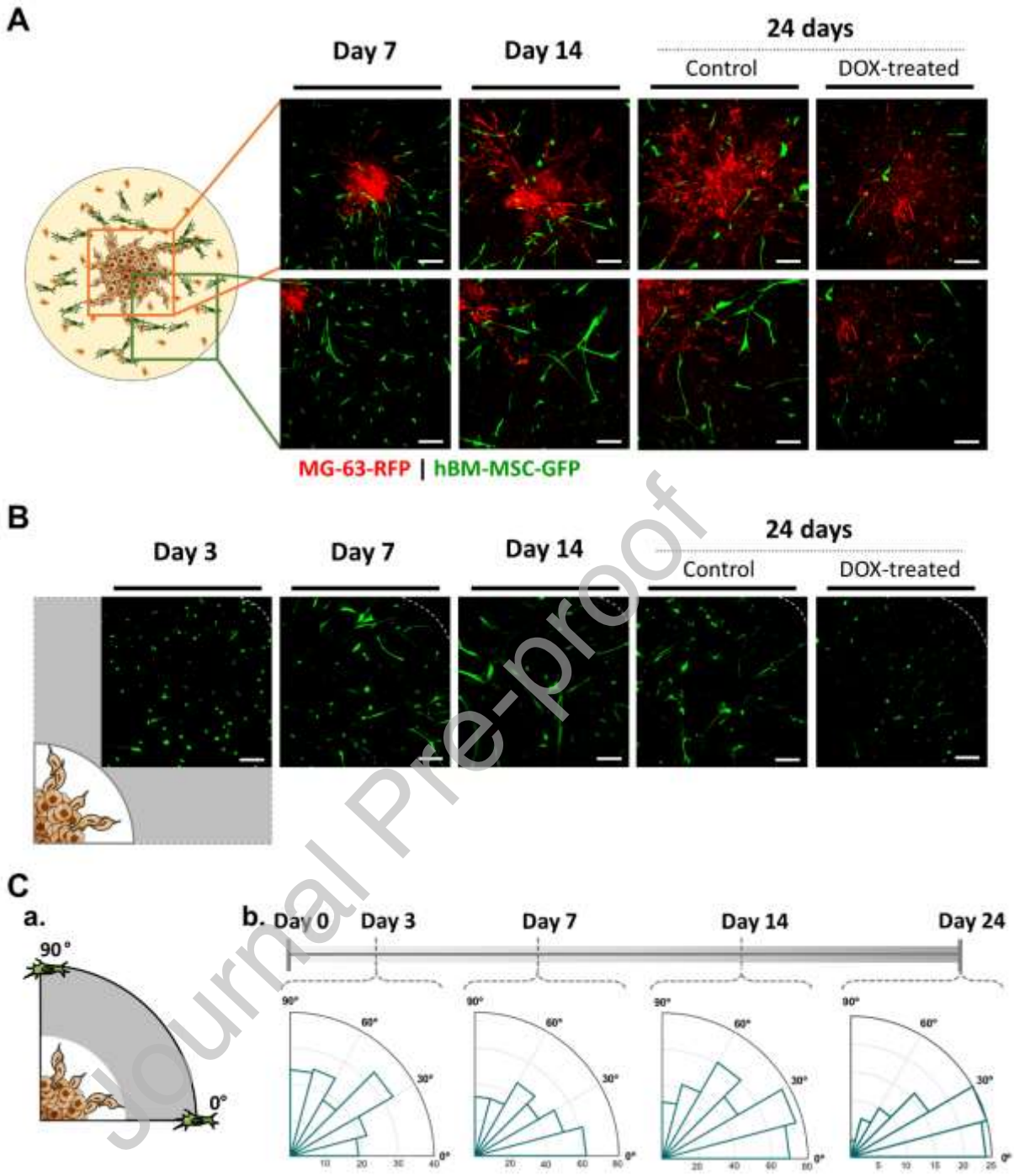

Figure 2. Tumor and stromal cell organization and direction in the co-culture model. Confocal microscopy images of control and DOX-treated (1.1 μM) co-culture model with fluorescent protein-transduced cells (MG-63-RFP, hBM-MSC-GFP) demonstrating (A) the synergistic interaction between MG-63 tumor cells and stem cells over the 24 days of culture and (B) the hBM-MSCs-GFP (green) stretching in hydrogel periphery towards OS spheroid center. Dashed lines are delimitating the hydrogel periphery. Scale

bar: 200 μm. (C) (a) Schematic representation of cell direction angle interpretation. The gray shaded region refers to the considered hydrogel zone for analysis, outside the invasive zone. (b) Distribution of stem cell direction angle at day 3, 7, 14 and 24, in controls. The x-axis and y-axis represent the frequency.

3.2. Doxorubicin dose-response of 3D OS models

The potential of the above-established OS models for drug development and screening was evaluated through a doxorubicin (DOX) dose-response testing, a commonly used anticancer agent in clinical OS therapy (Figure 3) [4]. To confirm drug availability inside PLMA hydrogel, a doxorubicin diffusivity test was performed, revealing a fast penetration of the drug in this protein mesh (Figure S7). The 3-day DOX treatment was initiated at 14 days of culture in order to allow a prior tumor spheroid growth, invasion and interaction with stromal cells in the PLMA hydrogels. Subsequently, at 24 days of culture, the mitochondrial metabolic activity was quantified using a colorimetric assay to determine the IC_{50}-value for each model, which is the drug concentration that inhibit a biological process by half. IC_{50}-values of scaffold-based models were compared to free-spheroid values, and the results showed that tumor cells were more sensitive to DOX treatment in the absence of an ECM-resemble matrix (Figure 3 and Table 1). Comparing with the IC_{50}-value of scaffold-free spheroids, the mono-culture and co-culture models were about 5-fold and 2.5-fold more resistant to DOX-induced death, respectively (Table 1). Interestingly, cells in the tri-culture model were 2-fold more sensitive to DOX compared to tumor spheroid embedded alone in the PLMA hydrogel.

The metabolic activity of scaffold-free and scaffold-based models in control and DOX-treated (1.1 μM) conditions were also compared (Figure S8). MG-63 cells of spheroid encapsulated in PLMA hydrogel demonstrated to have lower metabolic

activity than cells of free-spheroid. Moreover, the stromal cell combination with tumor spheroid resulted in a higher metabolic activity due to the larger number of cells cultured in the co-culture model, which is significantly different between control and DOX-treated groups of the other configurations. The non-significant difference between control and DOX-treated samples of the mono-culture model is in accordance with the highest IC_{50}-value aforementioned for the same model (Figure 3 and S8).

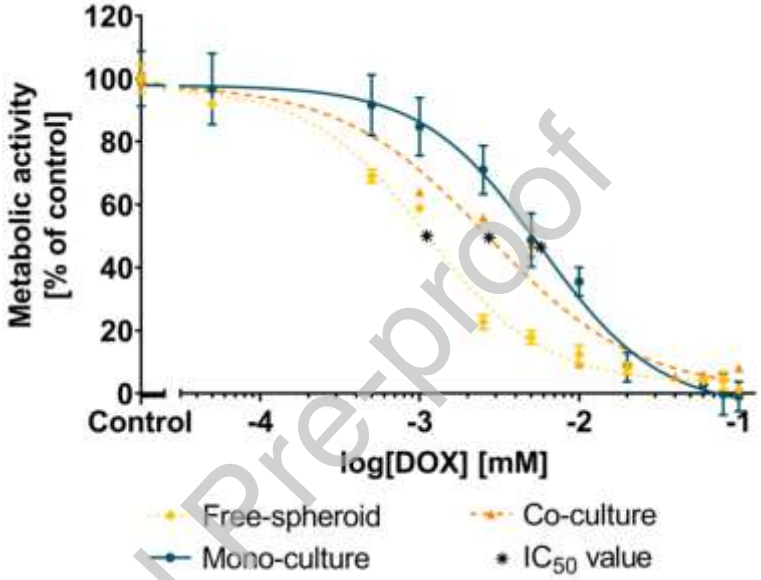

Figure 3. Effect of doxorubicin (DOX) on the established 3D OS models: scaffold-free spheroid and scaffold-based mono- and co-culture. Dose-response curves of DOX testing on OS models, determined through mitochondrial metabolic activity measurement at 24 days of culture, represented in percentage relatively to control. A non-linear regression of variable slope with four parameters of "log(inhibitor) vs. response", based on Equation (1), allowed the determination of the IC_{50}-values. Data are presented as mean ± SEM ($n \geq 3$).

Table 1. IC_{50}-values for the established 3D OS models. A 3-day DOX treatment was performed and the dose-dependent effect on cell metabolic activity was determined by IC_{50}-value calculation.

OS model setting	IC_{50}-value [μM]
Free-spheroid	1.10
Mono-culture	5.73
Co-culture	2.72

3.3. The role of ECM and stromal cells on doxorubicin cytotoxicity effect

3.3.1. Cell survival, morphology and spatial organization and bone-related matrix deposition

The live/dead assay showed the viability of the majority of the cells up to 24 days in the control conditions of all 3D configurations, evidencing the ability of the established models for long-term cell culture (Figure 4). Live/dead images of hBM-MSCs and FhOBs cultured alone confirmed the survival of these cell types encapsulated in PLMA hydrogels, similarly to co-culture model (Figure S6). Moreover, an increase of the invasive area in co-culture model compared with its mono-culture counterparts was evidenced. Regarding the DOX-treated samples, fluorescence images revealed that cells in the mono-culture models were more sensitive to drug exposure, particularly the tumor invasive branches of the PLMA-encapsulated spheroid. An increased cell viability in the co-culture model was detected, inclusively in the invasive branches. These evidences are confirmed by fluorescence images of the co-culture model with fluorescent protein-transduced cells, where most of the tumor cells were resistant to DOX treatment (Figure 2A and S2). Nevertheless, it was verified a significative cell death in the hydrogel periphery, as can be confirmed by a reduced number of hBM-MSC-GFP in DOX-treated samples in comparison to control (Figure 2A,B). The staining of actin filaments clearly demonstrated that cells in mono- and co-culture

control models proliferated from day 14 to 24 (Figure 5A). The death of tumor invasive cells in the mono-culture and the improved cell resistance in the co-culture model verified through live/dead staining are also confirmed by these fluorescence images. Moreover, the cell morphology assessment revealed that DOX-treated samples lost the interconnected network of stem cells visualized at the 14 and 24 days of culture in controls (Figure 2A,B and 5B). Tumor spheroid and stromal cell organization in the established 3D models were verified through histological analysis using hematoxylin and eosin staining (Figure S9).

The staining of calcium deposits by Alizarin Red demonstrated the formation of a mineralized matrix over the 24 days of culture. An increased calcium deposition in the control condition in comparison to DOX-treated samples was visualized, as well as a preferential deposition in the proliferative/invasive regions (Figure S10). A qualitative analysis of the expression of bone-related proteins, namely collagen, osteopontin and osteocalcin was also conducted (Figure S10 and S11). In the scaffold-free spheroids, an increasing in the production of the three bone-related proteins was observed from day 14 to day 24, being doxorubicin treatment responsible for a deregulation in their deposition. Contrary, a higher protein deposition in the mono-culture setting was verified at 14 days of culture, with a non-significative decrease up to 24 days of culture. Moreover, differences in proteins expression between control and doxorubicin treated samples were not observed, with the exception of collagen, which deposition increased in the presence of the drug. In the co-culture model, the production of these ic proteins was residual at 14 days of culture and at 24 days in doxorubicin-treated samples. However, in the control samples, it was observed collagen deposition in the proliferative and invasive regions, while osteocalcin and osteopontin was accumulated in the necrotic area of the tumor spheroid.

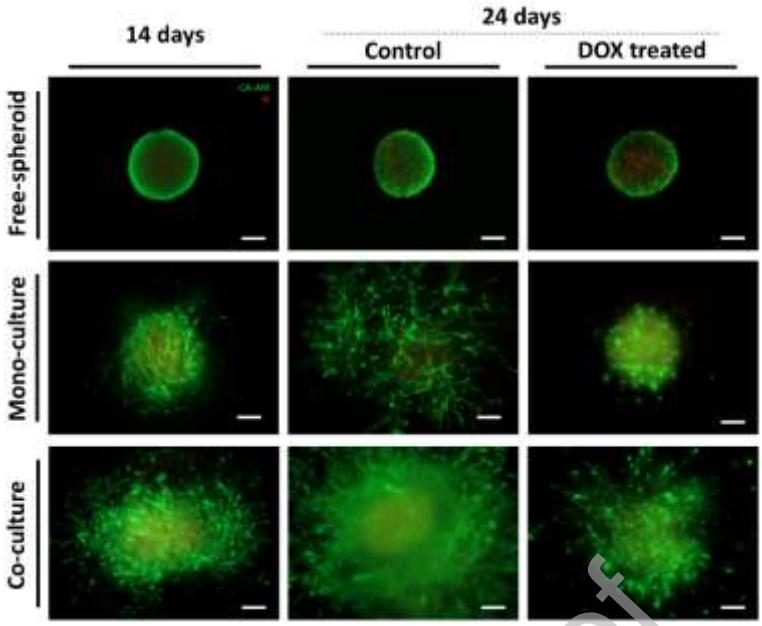

Figure 4. Fluorescence microscopy images of live/dead of the 3D OS models. Viability of MG-63 tumor spheroids cultured alone or in combination with hBM-MSCs and FhOBs at 14 and 24 days of culture. Cell sensitivity to a 3-day DOX treatment (1.1 μM) was analyzed at 24 days. The green and red channels represent the Calcein-AM (CA-AM) and PI staining of live and dead cells, respectively. Scale bar: 200 μm.

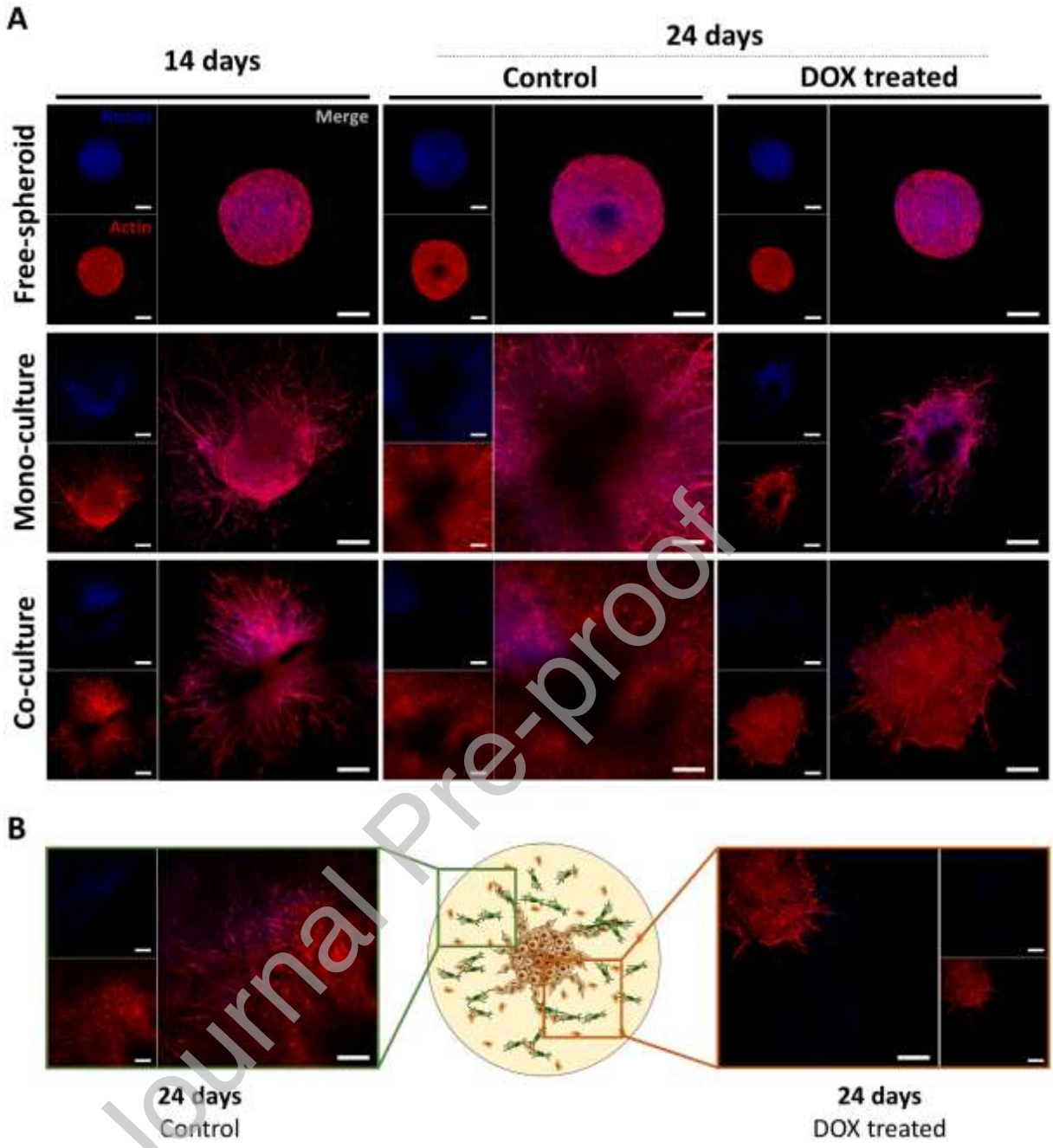

Figure 5. Fluorescence microscopy images of DAPI/Phalloidin staining of the established 3D models. (A) Cell morphology of the MG-63 tumor spheroids and surrounding stromal cells (hBM-MSCs and FhOBs) at 14 and 24 days of culture. Cell sensitivity to a 3-day doxorubicin treatment (1.1 μM) was analyzed at 24 days. (B) DAPI/Phalloidin images of the cellular network formed by hBM-MSCs and MG-63 tumor cells on control and DOX treated samples of co-culture model, at 24 days of

culture. Cells nuclei were stained by DAPI (blue) and F-actin filaments by phalloidin (red). Scale bar: 200 μm.

3.3.2. Tumor spheroid growth and invasiveness

Tumor growth and invasion are dynamic processes actively involved in metastasis development, which depend on the surrounding microenvironment [47]. MG-63 spheroid area changes, excluding the invaded area, were quantitatively analyzed in both models and the drug effect on this morphological feature was also evaluated. The compact structure of the initial spheroids was disturbed by cell outward movement from the spheroid and a more subtle increase in spheroid area was observed in the scaffold-based models, comparing to free-spheroid (Figure 6A). Comparing the control samples of the two PLMA-based models over the 24 days of culture, a more accentuated area increase was verified in the mono-culture model until the day 14. However, while in the co-culture the rate of area increase remained approximately constant, in the mono-culture a significant decrease in tumor growth was verified over time. With regard to the treated samples, a decrease in the spheroid area was observed in the mono-culture model, contrary to the co-culture model.

Cell invasiveness around tumor spheroid was also analyzed through fluorescence and optical contrast microscopy images acquired over time. Throughout most of the culture time, it was verified an increased length of invasive branches in the co-culture model, probably owing the integration of chemotactically interacting hBM-MSCs in tumor cell branches (Figure 6B). The treatment with DOX induced the death of some cells that constituted the invasive branches, an effect also visualized by cell invasiveness analysis. Nevertheless, tumor cells were more resistant to DOX treatment when in co-culture with tumor-associated stromal cells.

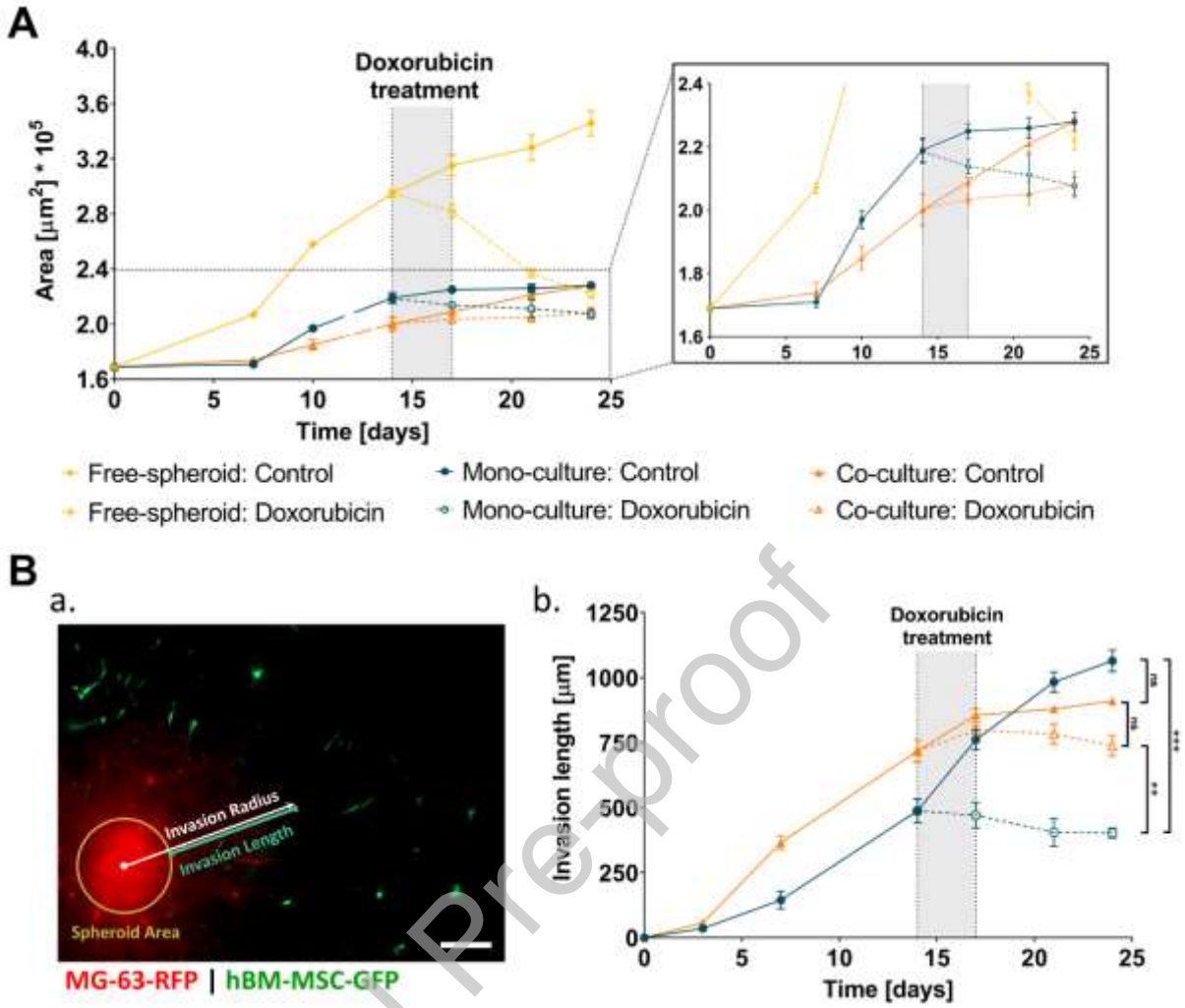

Figure 6. Spheroid growth and cell invasion in the 3D OS models. Progression of (A) spheroids area and (B) invasion length during the 24 days of culture, in control and DOX treated samples of the established models. The 3-day doxorubicin treatment (1.1 μM) is represented by the shaded region. Data are presented as mean ± SD ($n \geq 3$). *$p < 0.05$; **$p < 0.01$; ns – not significant.

4. Discussion

In this study, we developed a 3D *in vitro* OS invasion model based on the recognized potential of MCTS to recapitulate essential pathological properties of a tumor mass, such as the chemical gradients of oxygen and nutrients that support tumor survival [27]. Herein, MG-63 cell spheroids embedded into a human-derived matrix of

PLMA were co-cultured with human osteoblasts and hBM-MSCs. OS tumor cells were cultured to interact synergistically with the ECM-mimicking matrix and stromal cells that constitute the native bone microenvironment to enable the recapitulation of tumor growth and invasion. Moreover, their chemo-sensitivity was compared with spheroids cultured in a scaffold-free and scaffold-based mono-culture setting.

The understanding of the biochemical and mechanical mechanisms behind a disease development and the progress in biomimetic materials have opened new frontiers in the field of 3D *in vitro* disease modelling for the establishment of preclinical platforms with increased predictive value [9]. Particularly, advances in 3D tumor models for OS have been achieved in order to better recreate specific tumor microenvironmental cues not achievable with traditional 2D monolayer cultures [39,48]. Currently, MCTS is gaining momentum in cancer research as a scaffold-free platform, with the establishment of numerous 3D tumor models for drug screening [32,33,37,49–51]. Nevertheless, the tumor progression relies on cell invasion mechanisms, a critical event that precedes tumor metastasis development and is responsible for the poor-prognostic on the majority of patients [52]. Although scaffold-based models have contributed with fundamental knowledge of tumor pathology, only a few studies have reported matrix-embedded spheroids to evaluate the invasiveness of tumor cells in response to drug treatment before invasive branches arising [34,43]. However, the high frequency of advanced tumor stage upon diagnosis, with about 15-20% of patients presenting macroscopic metastasis and 80-90% assuming undetectable micrometastasis, evidences the emergency of new anticancer drug development that acts on invasive mechanisms [4,52]. It was on this scope that we herein explored a recently developed biomaterial of human origin, methacryloyl platelet-lysates (PLMA), to develop a disease model for invasive tumor chemosensitivity assessment [45]. The potential of

this scaffold to support distinct cell population culture and cell invasive behavior was clearly elucidated in a previous study, in which we reported a systematic analysis of cell spheroid viability, growth and invasiveness of four cell types into PLMA hydrogels with different stiffnesses [35]. The protein-rich content of human origin offers an unique bioactivity to produce cellular stimuli similar to native ones, an advantage over the traditionally used biomaterials of animal origin or derived from synthetic polymers [44,53]. In fact, rBM of murine EHS sarcoma (Matrigel®) and type I collagen, the most used natural biomaterials, present some shortcomings: they can trigger an *in vivo* immune response due to their animal origin; they exhibit poor mechanical properties; they are usually difficult to handle; and there are ethical issues related to animal testing and their welfare. Motivated by these drawbacks, much efforts have been made toward more sophisticated and cost-effective human-derived biomaterials which can be used not only to develop *in vitro* disease models, but also to explore *in vivo* applications not feasible with animal-derived materials. Tissue engineering and regenerative medicine are the main focus fields for human biomacromolecules application, leveraging the body's own mechanism orchestration to expedite *in situ* tissue repair and new tissue engineering [53]. However, their application in disease modeling for drug screening is very limited. [54] Given the important role of growth factors and other cytokines released from platelets in a variety of biological processes, including tumor growth, invasion, metastasis and drug resistance, the PLMA hydrogels resemble the natural microenvironment of tumors, being an appropriate platform for the development of disease models [55,56].

In the present study, three configurations of *in vitro* OS models were successfully developed: (i) scaffold-free tumor spheroids, and PLMA-embedded tumor spheroids (ii) alone or (iii) co-cultured with hBM-MSCs and FhOBs. MG-63 spheroid

were generated using the forced-floating technique which produce uniform and reproducible spheroids [28,31]. The generated MG-63 spheroids exhibited the heterogeneity attributed to *in vivo* solid avascular tumors, in which a well-defined chemical gradient of nutrients, oxygen and pH is established (Figure S1) [27]. Such microtissues developed a necrotic/hypoxic core and an external proliferative zone with metabolic active cells, validating their feasibility to be used throughout this study. To establish the scaffold-based models, the cell behaviors verified in our previous studies were taken into account, where similar MG-63 spheroids showed a higher invasion kinetics in softer hydrogels and stem cells revealed the preference for stiffer PLMA hydrogels [35,45]. Moreover, osteoblasts show a high cell viability and maintain the metabolic activity and gene expression when cultured in hydrogels with a stiffness ranging from 1.6 to 25 kPa [57]. Therefore, PLMA hydrogels at 15% (w/v), an intermediate condition in terms of mechanical properties (15 kPa), were used for the spheroid invasion models. Although PLMA hydrogel is softer than the bone tissue where OS develops, hydrogels have demonstrated to be great platforms for OS modelling [9]. Recognizing the importance of the instructive signals provided by stromal cells for tumor progression, we hypothesized that the synergistic interaction of an OS tumor with hBM-MSCs and FhOBs could recreate tumor growth and invasion. Effectively, several studies *in vitro* and *in vivo* have reported that MSCs migrate to OS tumor microenvironment in response to the release of soluble factors by tumor cells, playing a pivotal role in tumor survival, invasion and chemoresistance [21,58–60]. This tumor-stromal cell communication was clearly recapitulated through hBM-MSCs alignment toward OS tumor spheroid, as indicated by cell angle direction and stromal cell organization monitoring (Figure 2B,C and S5). Moreover, a network of stem cells directly interacting with invasive tumor cells was formed, stimulating the development

of a large invasive area (Figure 2A, 6 and S3). The cuboidal-to-round shape of osteoblasts (Figure S2B,C) is an evidence that FhOBs maintained their phenotype and did not differentiate into osteocytes, a process in which osteoblasts undergo morphological changes characterized by cell volume loss and elongation of thin cytoplasmic projections [61,62]. This observation can be related with the PLMA hydrogel mechanical properties, once it is reported that soft surfaces stimulate osteoblast-osteocyte differentiation in 2D and 3D settings, whereas on stiff surfaces as the herein used PLMA hydrogels, osteoblasts maintain their phenotypic cues [62]. In the herein studied 3D OS models, MG-63 tumor cells produced calcium deposits and collagens throughout the 24 days of culture, even in a small amount, also suggesting the formation of a bone-like environment (Figure S10). However, a different protein expression profile was verified for osteocalcin and osteopontin which were highly expressed in scaffold-free spheroid model by day 24 of culture, but whose expression in scaffold-based models was reduced, particularly in a co-culture setting (Figure S11). This protein expressing profile is related with the pre-osteoblastic phenotype of tumor cells. Effectively, osteosarcoma development is associated with genetic and epigenetic alterations that hamper the proper osteogenic differentiation of pre-osteoblasts [3,63]. As osteocalcin and osteopontin are late markers of bone formation, it was expected that MG-63 cell and non-differentiated hBM-MSCs evidenced low protein expression levels, as particularly verified in the co-culture model [63,64].

With the purpose of assess the potential of the established models as a drug screening platform, we evaluated the effects of a standard chemotherapeutic agent, doxorubicin, on cellular response. Not surprisingly, the 3D models herein established exhibited an increased resistance to DOX treatment comparing with 2D monolayer models reported in the literature for OS cell lines, 0.05-0.30 μM of DOX (Figure 3 and

Table 1) [29,30,33]. This chemoresistance are attributable to the above-discussed diffusion gradients in spheroids that limits drug diffusion and causes a preferential accumulation of drug at the periphery, similar to *in vivo* tumor microregions where necrotic areas develop [65–67]. Moreover, although chemotherapeutic drugs as DOX target high proliferative cells, it is known that tumor cells are able to develop multi-drug resistance mechanisms such as the over-expressing of membrane efflux pump proteins responsible for flushing out drugs [68]. We expected that the presence of an ECM-mimicking matrix surrounding the tumor spheroid would infer an increased resistance to drug-induced death when compared to scaffold-free spheroids counterparts. The 5-fold higher IC_{50}-value of mono-culture PLMA-encapsulated spheroid confirmed that assumption, a cell response that can be related with the invasive phenotype of tumor proliferating cells verified by the formation of invasion branches since the early days of culture (Figure 6). Other reason that can justify the reported drug resistance is the fact that encapsulated tumor cells underwent a decrease in their metabolic activity in response to matrix confinement, probably reducing drug metabolism (Figure S8) [69,70]. Besides the importance of ECM in tumor progression, we hypothesized that the presence of stromal cells, particularly of hBM-MSCs, would trigger pro-tumoral mechanisms by reducing the sensitivity of tumor cells to DOX exposure. In fact, tumor pathology is not merely attributed to tumor cells, being cellular and non-cellular components critical players in tumor initiation, growth and metastasis [71]. Recent studies on the culture of scaffold-free hetero-spheroids has demonstrated that the presence of stromal cells results in an enhanced drug resistance [72]. In a 3D setting similar to the described in the present study, Benton *et al.* reported that breast cancer spheroids cultured with stromal cells exhibit an enhanced resistance to drug treatment comparing to the mono-culture model [36]. However, this behavior was not evidenced

by metabolic activity measurement over the drug concentration range testing (Figure 3 and Table 1). In an attempt to understand these findings, cell viability, morphology, spatial organization, spheroid area and invasive length were investigated in a cytotoxicity testing, exposing the established 3D OS models to 1.1 μM of DOX. Qualitative analysis of cell viability staining and fluorescence microscopy of stably transduced MG-63-RFP and hBM-MSC-GFP suggests that tumor cells in the co-culture model were more resistant to DOX treatment than cells in the mono-culture model, particularly with regard to the invasive branches visible around the tumor spheroid (Figure 2, 4 and 6B). Nevertheless, comparing with the control sample at 24 days of culture, stromal cells of the hydrogel periphery were significantly affected by DOX (Figure 2A,B and 4). Actin filaments staining also revealed that sensitivity of stromal cells, which in the absence of DOX maintained the interconnective network previously verified at 14 days of culture (Figure 5B). These analysis from fluorescence images are correlated with metabolic activity results. A higher absorbance was showed both in control and DOX-treated co-culture samples due to the presence of a greater number of cells, however, a large difference was verified between these two conditions, supporting the above-mentioned sensitivity of stromal cells (Figure S8). These data strongly evidence that stromal cells were quite sensitive to DOX exposure, corroborating previously reported results that revealed hBM-MSCs apoptosis when exposed to a drug concentration (1 μM) and an exposure time (72h) similar to the present study [73]. Although the deleterious effect of DOX on MSCs remains unclear, some drug-mediated cellular events were reported, such as low cell proliferation, cell shrinkage, enhanced reactive oxygen species production, mitochondrial membrane damage and hindering of cardiomyogenic differentiation [73,74]. Hence, the lower IC_{50}-value of co-culture model compared with mono-culture counterparts can be largely related with stromal cell death.

Although these findings, the assessment of spheroid area and invasive length, in conjugation with a qualitative fluorescence images analysis, are indicators of the pro-tumoral role exerted by hBM-MSCs in the co-culture model. Fluorescence images of stably transduced cells suggest that stem cells enhanced the formation of invasive branches around tumor spheroid, a data confirmed by invasion length quantification (Figure 2 and 6B). Moreover, it was verified a linear growth of the compact spheroid mass area over the 24 days of culture in the control, alongside the maintenance of spheroid area after DOX treatment (Figure 6A). Combined, these data evidence the protective role of hBM-MSCs, promoting tumor growth and the development of an increased invasive area. As aforementioned, the pro-tumoral role of MSCs in tumor progression is of general consensus [25]. In this sense, we believe that the established 3D co-culture model can be applied for drug screening and development and to study new approaches to optimize the drug delivery to *in vivo* tumors. Some strategies concern the re-education of MSCs to inhibit their migration to tumor microenvironment or use them as "trojan horses", exploring the integration mechanisms of MSCs in the tumor environment to develop cell-mediated therapies, have been of great interest in tumor research community [25,65,75,76]. In fact, several *in vitro* and *in vivo* studies exploring these approaches of MSC-mediated therapies have been promising to target bone cancer progression [58,59,77,78]. Taking advantage of the human protein-rich content of PLMA hydrogels, these scaffold-based models can also be explored to develop strategies of targeting the ECM in order to facilitate the diffusion of therapeutic agents into the tumor microenvironment [71,79].

The herein presented study highlights the potential of PLMA-based hydrogel for the development of humanized 3D *in vitro* disease modeling for drug screening purposes. The successful long-term culture (24 days) of tumor cell synergistically

interacting with two stromal cell types is an evident advantage of the developed 3D models over the 2D monolayer cultures. Moreover, the biomaterial's mechanical integrity over time, alongside with its cost-effective human origin, reinforce the idea that PLMA hydrogels are a great alternative to the "gold standards" for 3D disease modeling, rBM of EHS sarcoma and type I collagen. Inclusively, to the best of our knowledge, this is the first study reporting the development of a 3D tri-culture tumor model using a human-derived matrix.

5. Conclusion

The progress in 3D *in vitro* OS models have provided fundamental insights regarding the biomechanical bone-specific cues and chemoresistance mechanisms. Encouraged by the emergency of new therapeutic agents to target metastasis events, we developed a humanized 3D *in vitro* OS invasion model of MG-63 tumor spheroids embedded in human-derived PLMA hydrogels, co-cultured with FhOBs and hBM-MSCs. Tumor cell behavior in the presence of stromal cells was compared with two configurations of mono-culture models: a scaffold-free approach and a scaffold-based approach in which tumor spheroid was embedded in PLMA hydrogel alone. The integration of stromal cells in the surrounding microenvironment of the tumor revealed to recapitulate the chemotactically attraction exerted by tumor cells in hBM-MSCs. This synergistic tumor-stromal cell interaction triggered a positive outcome in OS tumor in terms of growth, invasive ability and improved resistance to doxorubicin treatment, revealing the potential of the herein established co-culture model as a reliable platform for drug screening purposes. The accurate recapitulation of the tumor invasion events opens up the possibility of exploring potential therapeutic strategies, contributing for the development and preclinical validation of new drugs to prevent the formation of

micrometastasis, one of the main concerns associated with cancer treatment. Furthermore, the remarkable bioactive and mechanical support provided by PLMA hydrogels offer a relevant humanized platform with the potential to predict patients' response and expedite the availability of effective therapies for numerous pathologies.

Acknowledgements

This work was developed within the scope of the project CICECO-Aveiro Institute of Materials, UIDB/50011/2020 & UIDP/50011/2020, financed by national funds through the Foundation for Science and Technology/MCTES. The authors would like to acknowledge the support of the European Research Council Proof-of-Concept Grant Agreement No. ERC-2017-PoC-789760 for the project MicroBone. This work was also supported by the Fundation for Science and Technology through the individual contract CEECIND/02713/2017 of Dr. Catarina A. Custódio and the doctoral grant SFRH/BD/144640/2019 of Cátia F. Monteiro.

Image acquisition was performed in the LiM facility of iBiMED, a node of PPBI (Portuguese Platform of BioImaging): POCI-01-0145-FEDER-022122.

Declaration of Competing Interest

The authors declare that they have no known competing financial interests or personal relationships that could have appeared to influence the work reported in this paper.

Declaration of interests

☒ The authors declare that they have no known competing financial interests or personal relationships that could have appeared to influence the work reported in this paper.

☐The authors declare the following financial interests/personal relationships which may be considered as potential competing interests:

References

[1] L. Mirabello, R.J. Troisi, S.A. Savage, Osteosarcoma incidence and survival rates from 1973 to 2004: Data from the Surveillance, Epidemiology, and End Results Program, Cancer. 115 (2009) 1531–1543. https://doi.org/10.1002/cncr.24121.

[2] A. Alfranca, L. Martinez-Cruzado, J. Tornin, A. Abarrategi, T. Amaral, E. de Alava, P. Menendez, J. Garcia-Castro, R. Rodriguez, Bone microenvironment signals in osteosarcoma development, Cell. Mol. Life Sci. 72 (2015) 3097–3113. https://doi.org/10.1007/s00018-015-1918-y.

[3] A. Abarrategi, J. Tornin, L. Martinez-Cruzado, A. Hamilton, E. Martinez-Campos, J.P. Rodrigo, M.V. González, N. Baldini, J. Garcia-Castro, R. Rodriguez, Osteosarcoma: Cells-of-Origin, Cancer Stem Cells, and Targeted Therapies, Stem Cells Int. 2016 (2016) 1–13. https://doi.org/10.1155/2016/3631764.

[4] A. Luetke, P.A. Meyers, I. Lewis, H. Juergens, Osteosarcoma treatment – Where do we stand? A state of the art review, Cancer Treat. Rev. 40 (2014) 523–532. https://doi.org/10.1016/j.ctrv.2013.11.006.

[5] D.J. Harrison, C.L. Schwartz, Osteogenic Sarcoma: Systemic Chemotherapy Options for Localized Disease, Curr. Treat. Options Oncol. 18 (2017) 24. https://doi.org/10.1007/s11864-017-0464-2.

[6] D.J. Harrison, D.S. Geller, J.D. Gill, V.O. Lewis, R. Gorlick, Current and future therapeutic approaches for osteosarcoma, Expert Review of Anticancer Therapy. 18 (2018) 39–50. https://doi.org/10.1080/14737140.2018.1413939.

[7] C.M. Hattinger, M.P. Patrizio, F. Magagnoli, S. Luppi, M. Serra, An update on emerging drugs in osteosarcoma: towards tailored therapies?, Expert Opinion on Emerging Drugs. 24 (2019) 153–171. https://doi.org/10.1080/14728214.2019.1654455.

[8] P. Horvath, N. Aulner, M. Bickle, A.M. Davies, E.D. Nery, D. Ebner, M.C. Montoya, P. Östling, V. Pietiäinen, L.S. Price, S.L. Shorte, G. Turcatti, C. von Schantz, N.O. Carragher, Screening out irrelevant cell-based models of disease, Nat Rev Drug Discov. 15 (2016) 751–769. https://doi.org/10.1038/nrd.2016.175.

[9] T. Chow, I. Wutami, E. Lucarelli, P.F. Choong, S. Duchi, C. Di Bella, Creating In Vitro Three-Dimensional Tumor Models: A Guide for the Biofabrication of a Primary Osteosarcoma Model, Tissue Engineering Part B: Reviews. (2020) ten.teb.2020.0254. https://doi.org/10.1089/ten.teb.2020.0254.

[10] I. Corre, F. Verrecchia, V. Crenn, F. Redini, V. Trichet, The Osteosarcoma Microenvironment: A Complex but Targetable Ecosystem, Cells. 9 (2020) 976. https://doi.org/10.3390/cells9040976.

[11] E.R. Molina, L.K. Chim, S. Barrios, J.A. Ludwig, A.G. Mikos, Modeling the Tumor Microenvironment and Pathogenic Signaling in Bone Sarcoma, Tissue Engineering Part B: Reviews. 26 (2020) 249–271. https://doi.org/10.1089/ten.teb.2019.0302.

[12] I. Levinger, Y. Ventura, R. Vago, Life is Three Dimensional-As In Vitro Cancer Cultures Should Be, Adv. Cancer Res. 121 (2014) 383–414. https://doi.org/10.1016/B978-0-12-800249-0.00009-3.

[13] K.A. Fitzgerald, M. Malhotra, C.M. Curtin, F.J. O' Brien, C.M. O' Driscoll, Life in 3D is never flat: 3D models to optimise drug delivery, J. Controlled Release. 215 (2015) 39–54. https://doi.org/10.1016/j.jconrel.2015.07.020.

[14] N. Shologu, E. Szegezdi, A. Lowery, M. Kerin, A. Pandit, D.I. Zeugolis, Recreating complex pathophysiologies in vitro with extracellular matrix surrogates for anticancer therapeutics screening, Drug Discovery Today. 21 (2016) 1521–1531. https://doi.org/10.1016/j.drudis.2016.06.001.

[15] H.T. Aiyelabegan, E. Sadroddiny, Fundamentals of protein and cell interactions in biomaterials, Biomed. Pharmacother. 88 (2017) 956–970. https://doi.org/10.1016/j.biopha.2017.01.136.

[16] A.W. Lambert, D.R. Pattabiraman, R.A. Weinberg, Emerging Biological Principles of Metastasis, Cell. 168 (2017) 670–691. https://doi.org/10.1016/j.cell.2016.11.037.

[17] V. Gkretsi, T. Stylianopoulos, Cell Adhesion and Matrix Stiffness: Coordinating Cancer Cell Invasion and Metastasis, Front. Oncol. 8 (2018) 145. https://doi.org/10.3389/fonc.2018.00145.

[18] M.R. Junttila, F.J. de Sauvage, Influence of tumour micro-environment heterogeneity on therapeutic response, Nature. 501 (2013) 346–354. https://doi.org/10.1038/nature12626.

[19] E.L.S. Fong, D.A. Harrington, M.C. Farach-Carson, H. Yu, Heralding a new paradigm in 3D tumor modeling, Biomaterials. 108 (2016) 197–213. https://doi.org/10.1016/j.biomaterials.2016.08.052.

[20] G. Lazennec, P.Y. Lam, Recent discoveries concerning the tumor - mesenchymal stem cell interactions, Biochim. Biophys. Acta, Rev. Cancer. 1866 (2016) 290–299. https://doi.org/10.1016/j.bbcan.2016.10.004.

[21] M. Cortini, A. Massa, S. Avnet, G. Bonuccelli, N. Baldini, Tumor-activated mesenchymal stromal cells promote osteosarcoma stemness and migratory potential via IL-6 secretion, PLoS One. 11 (2016) e0166500. https://doi.org/10.1371/journal. pone.0166500.

[22] L.P. Ferreira, V.M. Gaspar, R. Henrique, C. Jerónimo, J.F. Mano, Mesenchymal Stem Cells Relevance in Multicellular Bioengineered 3D In Vitro Tumor Models, Biotechnol. J. 12 (2017) 1700079. https://doi.org/10.1002/biot.201700079.

[23] M. Cortini, S. Avnet, N. Baldini, Mesenchymal stroma: Role in osteosarcoma progression, Cancer Letters. 405 (2017) 90–99. https://doi.org/10.1016/j.canlet.2017.07.024.

[24] S. Duchi, G. Sotgiu, E. Lucarelli, M. Ballestri, B. Dozza, S. Santi, A. Guerrini, P. Dambruoso, S. Giannini, D. Donati, C. Ferroni, G. Varchi, Mesenchymal stem cells as delivery vehicle of porphyrin loaded nanoparticles: effective photoinduced in vitro killing of osteosarcoma, J Control Release. 168 (2013) 225–237. https://doi.org/10.1016/j.jconrel.2013.03.012.

[25] Y. Shi, L. Du, L. Lin, Y. Wang, Tumour-associated mesenchymal stem/stromal cells: emerging therapeutic targets, Nat. Rev. Drug Discovery. 16 (2017) 35–52. https://doi.org/10.1038/nrd.2016.193.

[26] Y. Zheng, G. Wang, R. Chen, Y. Hua, Z. Cai, Mesenchymal stem cells in the osteosarcoma microenvironment: their biological properties, influence on tumor growth, and therapeutic implications, Stem Cell Res. Ther. 9 (2018) 22. https://doi.org/10.1186/s13287-018-0780-x.

[27] M. Chatzinikolaidou, Cell spheroids: the new frontiers in in vitro models for cancer drug validation, Drug Discovery Today. 21 (2016) 1553–1560. https://doi.org/10.1016/j.drudis.2016.06.024.

[28] T.J. Puls, X. Tan, M. Husain, C.F. Whittington, M.L. Fishel, S.L. Voytik-Harbin, Development of a Novel 3D Tumor-tissue Invasion Model for High-throughput, High-content Phenotypic Drug Screening, Sci. Rep. 8 (2018) 13039. https://doi.org/10.1038/s41598-018-31138-6.

[29] K. Arai, R. Sakamoto, D. Kubota, T. Kondo, Proteomic approach toward molecular backgrounds of drug resistance of osteosarcoma cells in spheroid culture

system, Proteomics. 13 (2013) 2351–2360. https://doi.org/10.1002/pmic.201300053.

[30] M. Rimann, S. Laternser, A. Gvozdenovic, R. Muff, B. Fuchs, J.M. Kelm, U. Graf-Hausner, An in vitro osteosarcoma 3D microtissue model for drug development, J. Biotechnol. 189 (2014) 129–135. https://doi.org/10.1016/j.jbiotec.2014.09.005.

[31] A.I. Neto, C.R. Correia, M.B. Oliveira, M.I. Rial-Hermida, C. Alvarez-Lorenzo, R.L. Reis, J.F. Mano, A novel hanging spherical drop system for the generation of cellular spheroids and high throughput combinatorial drug screening, Biomater. Sci. 3 (2015) 581–585. https://doi.org/10.1039/c4bm00411f.

[32] N. Baek, O.W. Seo, J. Lee, J. Hulme, S.S.A. An, Real-time monitoring of cisplatin cytotoxicity on three-dimensional spheroid tumor cells, Drug Des., Dev. Ther. 10 (2016) 2155–2165. https://doi.org/10.2147/DDDT.S108004.

[33] N. Baek, O.W. Seo, M. Kim, J. Hulme, S.S.A. An, Monitoring the effects of doxorubicin on 3D-spheroid tumor cells in real-time, OncoTargets Ther. 9 (2016) 7207–7218. https://doi.org/10.2147/OTT.S112566.

[34] M. Pavlou, M. Shah, P. Gikas, T. Briggs, S.J. Roberts, U. Cheema, Osteomimetic matrix components alter cell migration and drug response in a 3D tumour-engineered osteosarcoma model, Acta Biomater. 96 (2019) 247–257. https://doi.org/10.1016/j.actbio.2019.07.011.

[35] C.F. Monteiro, S.C. Santos, C.A. Custódio, J.F. Mano, Human Platelet Lysates-Based Hydrogels: A Novel Personalized 3D Platform for Spheroid Invasion Assessment, Adv. Sci. 7 (2020) 1902398. https://doi.org/10.1002/advs.201902398.

[36] G. Benton, G. DeGray, H.K. Kleinman, J. George, I. Arnaoutova, In Vitro Microtumors Provide a Physiologically Predictive Tool for Breast Cancer

Therapeutic Screening, PLOS ONE. 10 (2015) e0123312. https://doi.org/10.1371/journal.pone.0123312.

[37] M.G. McCoy, D. Nyanyo, C.K. Hung, J.P. Goerger, W.R. Zipfel, R.M. Williams, N. Nishimura, C. Fischbach, Endothelial cells promote 3D invasion of GBM by IL-8-dependent induction of cancer stem cell properties, Sci. Rep. 9 (2019) 9069. https://doi.org/10.1038/s41598-019-45535-y.

[38] B. Kundu, A.R.F. Bastos, V. Brancato, M.T. Cerqueira, J.M. Oliveira, V.M. Correlo, R.L. Reis, S.C. Kundu, Mechanical Property of Hydrogels and the Presence of Adipose Stem Cells in Tumor Stroma Affect Spheroid Formation in the 3D Osteosarcoma Model, ACS Appl. Mater. Interfaces. 11 (2019) 14548–14559. https://doi.org/10.1021/acsami.8b22724.

[39] C.F. Monteiro, C.A. Custódio, J.F. Mano, Three-Dimensional Osteosarcoma Models for Advancing Drug Discovery and Development, Adv. Ther. 2 (2018) 1800108. https://doi.org/10.1002/adtp.201800108.

[40] E.C. González Díaz, S. Sinha, R.S. Avedian, F. Yang, Tissue-engineered 3D models for elucidating primary and metastatic bone cancer progression, Acta Biomaterialia. 99 (2019) 18–32. https://doi.org/10.1016/j.actbio.2019.08.020.

[41] K.M. Charoen, B. Fallica, Y.L. Colson, M.H. Zaman, M.W. Grinstaff, Embedded multicellular spheroids as a biomimetic 3D cancer model for evaluating drug and drug-device combinations, Biomaterials. 35 (2014) 2264–2271. https://doi.org/10.1016/j.biomaterials.2013.11.038.

[42] P. Techavichit, Y. Gao, L. Kurenbekova, R. Shuck, L.A. Donehower, J.T. Yustein, Secreted Frizzled-Related Protein 2 (sFRP2) promotes osteosarcoma invasion and metastatic potential, BMC Cancer. 16 (2016) 869. https://doi.org/10.1186/s12885-016-2909-6.

[43] V.M. Wu, J. Mickens, V. Uskoković, Bisphosphonate-Functionalized Hydroxyapatite Nanoparticles for the Delivery of the Bromodomain Inhibitor JQ1 in the Treatment of Osteosarcoma, ACS Appl. Mater. Interfaces. 9 (2017) 25887–25904. https://doi.org/10.1021/acsami.7b08108.

[44] S.C. Santos, Ó.E. Sigurjonsson, C.A. Custódio, J.F. Mano, Blood Plasma Derivatives for Tissue Engineering and Regenerative Medicine Therapies, Tissue Eng., Part B. 24 (2018) 454. https://doi.org/10.1089/ten.TEB.2018.0008.

[45] S.C. Santos, C.A. Custódio, J.F. Mano, Photopolymerizable Platelet Lysate Hydrogels for Customizable 3D Cell Culture Platforms, Adv. Healthcare Mater. 7 (2018) 1800849. https://doi.org/10.1002/adhm.201800849.

[46] W. Chen, C. Wong, E. Vosburgh, A.J. Levine, D.J. Foran, E.Y. Xu, High-throughput Image Analysis of Tumor Spheroids: A User-friendly Software Application to Measure the Size of Spheroids Automatically and Accurately, J. Visualized Exp. 8 (2014) e51639. https://doi.org/10.3791/51639.

[47] M. Lintz, A. Muñoz, C.A. Reinhart-King, The mechanics of single cell and collective migration of tumor cells, J. Biomech. Eng. 139 (2017) 021005. https://doi.org/10.1115/1.4035121.

[48] M. Cortini, N. Baldini, S. Avnet, New Advances in the Study of Bone Tumors: A Lesson From the 3D Environment, Front. Physiol. 10 (2019) 814. https://doi.org/10.3389/fphys.2019.00814.

[49] L.P. Ferreira, V.M. Gaspar, J.F. Mano, Bioinstructive microparticles for self-assembly of mesenchymal stem Cell-3D tumor spheroids, Biomaterials. 185 (2018) 155–173. https://doi.org/10.1016/j.biomaterials.2018.09.007.

[50] Z. Zhang, H. Wang, Q. Ding, Y. Xing, Z. Xu, C. Lu, D. Luo, L. Xu, W. Xia, C. Zhou, M. Shi, Establishment of patient-derived tumor spheroids for non-small cell

lung cancer, PLoS ONE. 13 (2018) e0194016. https://doi.org/10.1371/journal.pone.0194016.

[51] E. Folkesson, B. Niederdorfer, V.T. Nakstad, L. Thommesen, G. Klinkenberg, A. Lægreid, Å. Flobak, High-throughput screening reveals higher synergistic effect of MEK inhibitor combinations in colon cancer spheroids, Sci. Rep. 10 (2020) 11574. https://doi.org/10.1038/s41598-020-68441-0.

[52] C. Meazza, P. Scanagatta, Metastatic osteosarcoma: a challenging multidisciplinary treatment, Expert Rev. Anticancer Ther. 16 (2016) 543–556. https://doi.org/10.1586/14737140.2016.1168697.

[53] F.M. Chen, X. Liu, Advancing biomaterials of human origin for tissue engineering, Prog. Polym. Sci. 53 (2016) 86. https://doi.org/10.1016/j.progpolymsci.2015.02.004.

[54] S.D. Sackett, D.M. Tremmel, F. Ma, A.K. Feeney, R.M. Maguire, M.E. Brown, Y. Zhou, X. Li, C. O'Brien, L. Li, W.J. Burlingham, J.S. Odorico, Extracellular matrix scaffold and hydrogel derived from decellularized and delipidized human pancreas, Sci. Rep. 8 (2018) 10452. https://doi.org/10.1038/s41598-018-28857-1.

[55] B. Tesfamariam, Involvement of platelets in tumor cell metastasis, Pharmacol. Ther. 157 (2016) 112–119. https://doi.org/10.1016/j.pharmthera.2015.11.005.

[56] P. Huong, L. Nguyen, X.-B. Nguyen, S. Lee, D.-H. Bach, The Role of Platelets in the Tumor-Microenvironment and the Drug Resistance of Cancer Cells, Cancers. 11 (2019) 240. https://doi.org/10.3390/cancers11020240.

[57] T. Jiang, J. Zhao, S. Yu, Z. Mao, C. Gao, Y. Zhu, C. Mao, L. Zheng, Untangling the response of bone tumor cells and bone forming cells to matrix stiffness and adhesion ligand density by means of hydrogels, Biomaterials. 188 (2019) 130–143. https://doi.org/10.1016/j.biomaterials.2018.10.015.

[58] X. Duan, H. Guan, Y. Cao, E.S. Kleinerman, Murine bone marrow-derived mesenchymal stem cells as vehicles for interleukin-12 gene delivery into Ewing sarcoma tumors: IL-12 Gene Delivery Into Tumors by MSCs, Cancer. 115 (2009) 13–22. https://doi.org/10.1002/cncr.24013.

[59] B. Qiao, W. Shui, L. Cai, S. Guo, D. Jiang, Human mesenchymal stem cells as delivery of osteoprotegerin gene: homing and therapeutic effect for osteosarcoma, Drug Des., Dev. Ther. 9 (2015) 969–976. https://doi.org/10.2147/DDDT.S77116.

[60] S. Kalimuthu, L. Zhu, J.M. Oh, P. Gangadaran, H.W. Lee, S. hwan Baek, R.L. Rajendran, A. Gopal, S.Y. Jeong, S.-W. Lee, J. Lee, B.-C. Ahn, Migration of mesenchymal stem cells to tumor xenograft models and *in vitro* drug delivery by doxorubicin, Int. J. Med. Sci. 15 (2018) 1051–1061. https://doi.org/10.7150/ijms.25760.

[61] C.A. Mullen, M.G. Haugh, M.B. Schaffler, R.J. Majeska, L.M. McNamara, Osteocyte differentiation is regulated by extracellular matrix stiffness and intercellular separation, J. Mech. Behav. Biomed. Mater. 28 (2013) 183–194. https://doi.org/10.1016/j.jmbbm.2013.06.013.

[62] M.J. Mc Garrigle, C.A. Mullen, M.G. Haugh, M.C. Voisin, L.M. McNamara, Osteocyte differentiation and the formation of an interconnected cellular network in vitro, Eur. Cells Mater. 31 (2016) 323–340. https://doi.org/10.22203/eCM.v031a21.

[63] E.R. Wagner, G. Luther, G. Zhu, Q. Luo, Q. Shi, S.H. Kim, J.-L. Gao, E. Huang, Y. Gao, K. Yang, L. Wang, C. Teven, X. Luo, X. Liu, M. Li, N. Hu, Y. Su, Y. Bi, B.-C. He, N. Tang, J. Luo, L. Chen, G. Zuo, R. Rames, R.C. Haydon, H.H. Luu, T.-C. He, Defective Osteogenic Differentiation in the Development of Osteosarcoma, Sarcoma. 2011 (2011) 1–12. https://doi.org/10.1155/2011/325238.

[64] X. Han, W. Wang, J. He, L. Jiang, X. Li, Osteopontin as a biomarker for osteosarcoma therapy and prognosis, Oncol. Lett. 17 (2019) 2592–2598. https://doi.org/10.3892/ol.2019.9905.

[65] H. Lu, M.H. Stenzel, Multicellular Tumor Spheroids (MCTS) as a 3D In Vitro Evaluation Tool of Nanoparticles, Small. 14 (2018) 1702858. https://doi.org/10.1002/smll.201702858.

[66] C. Eilenberger, M. Rothbauer, E.-K. Ehmoser, P. Ertl, S. Küpcü, Effect of Spheroidal Age on Sorafenib Diffusivity and Toxicity in a 3D HepG2 Spheroid Model, Sci. Rep. 9 (2019) 4863. https://doi.org/10.1038/s41598-019-41273-3.

[67] A. Tchoryk, V. Taresco, R.H. Argent, M. Ashford, P.R. Gellert, S. Stolnik, A. Grabowska, M.C. Garnett, Penetration and Uptake of Nanoparticles in 3D Tumor Spheroids, Bioconjugate Chem. 30 (2019) 1371–1384. https://doi.org/10.1021/acs.bioconjchem.9b00136.

[68] Q. Wu, Z. Yang, Y. Nie, Y. Shi, D. Fan, Multi-drug resistance in cancer chemotherapeutics: Mechanisms and lab approaches, Cancer Lett. 347 (2014) 159–166. https://doi.org/10.1016/j.canlet.2014.03.013.

[69] A.C. Luca, S. Mersch, R. Deenen, S. Schmidt, I. Messner, K.-L. Schäfer, S.E. Baldus, W. Huckenbeck, R.P. Piekorz, W.T. Knoefel, A. Krieg, N.H. Stoecklein, Impact of the 3D Microenvironment on Phenotype, Gene Expression, and EGFR Inhibition of Colorectal Cancer Cell Lines, PLoS ONE. 8 (2013) e59689. https://doi.org/10.1371/journal.pone.0059689.

[70] S. Russell, J. Wojtkowiak, A. Neilson, R.J. Gillies, Metabolic Profiling of healthy and cancerous tissues in 2D and 3D, Sci Rep. 7 (2017) 15285. https://doi.org/10.1038/s41598-017-15325-5.

[71] K.C. Valkenburg, A.E. de Groot, K.J. Pienta, Targeting the tumour stroma to improve cancer therapy, Nat. Rev. Clin. Oncol. 15 (2018) 366–381. https://doi.org/10.1038/ s41571-018-0007-1.

[72] V. Brancato, F. Gioiella, G. Imparato, D. Guarnieri, F. Urciuolo, P.A. Netti, 3D breast cancer microtissue reveals the role of tumor microenvironment on the transport and efficacy of free-doxorubicin in vitro, Acta Biomater. 75 (2018) 200–212. https://doi.org/10.1016/j.actbio.2018.05.055.

[73] F. Yang, H. Chen, Y. Liu, K. Yin, Y. Wang, X. Li, G. Wang, S. Wang, X. Tan, C. Xu, Y. Lu, B. Cai, Doxorubicin Caused Apoptosis of Mesenchymal Stem Cells via p38, JNK and p53 Pathway, Cell. Physiol. Biochem. 32 (2013) 1072–1082. https://doi.org/10.1159/000354507.

[74] M.S. Oliveira, J.L. Carvalho, A.C.D.A. Campos, D.A. Gomes, A.M. de Goes, M.M. Melo, Doxorubicin has in vivo toxicological effects on ex vivo cultured mesenchymal stem cells, Toxicol. Lett. 224 (2014) 380–386. https://doi.org/10.1016/j.toxlet.2013.11.023.

[75] J. Zhang, J. Liu, Tumor stroma as targets for cancer therapy, Pharmacol. Ther. 137 (2013) 200–215. https://doi.org/10.1016/j.pharmthera.2012.10.003.

[76] M. Millard, I. Yakavets, V. Zorin, A. Kulmukhamedova, S. Marchal, L. Bezdetnaya, Drug delivery to solid tumors: the predictive value of the multicellular tumor spheroid model for nanomedicine screening, Int. J. Nanomed. 12 (2017) 7993–8007. https://doi.org/10.2147/IJN.S146927.

[77] Q.-A. NguyenThai, N. Sharma, D.H. Luong, S.S. Sodhi, J.-H. Kim, N. Kim, S.-J. Oh, D.K. Jeong, Targeted inhibition of osteosarcoma tumor growth by bone marrow-derived mesenchymal stem cells expressing cytosine deaminase/5-

fluorocytosine in tumor-bearing mice: Anti-tumor activity of CD/5FC-MSCs, J. Gene Med. 17 (2015) 87–99. https://doi.org/10.1002/jgm.2826.

[78] R. Fontanella, A. Pelagalli, A. Nardelli, C. D'Alterio, C. Ieranò, L. Cerchia, E. Lucarelli, S. Scala, A. Zannetti, A novel antagonist of CXCR4 prevents bone marrow-derived mesenchymal stem cell-mediated osteosarcoma and hepatocellular carcinoma cell migration and invasion, Cancer Lett. 370 (2016) 100–107. https://doi.org/10.1016/j.canlet.2015.10.018.

[79] M.R. Villegas, A. Baeza, M. Vallet-Regí, Hybrid Collagenase Nanocapsules for Enhanced Nanocarrier Penetration in Tumoral Tissues, ACS Appl. Mater. Interfaces. 7 (2015) 24075–24081. https://doi.org/10.1021/acsami.5b07116.

Graphical abstract